A novel fast and low-cost masonry monitoring strategy and application on arches

A novel fast and low-cost masonry monitoring strategy and application on arches

Gabriel Stockdale [(1)], Yu Yuan [(2)], Gabriele Milani [(2)*]
(1) Masonry Methods, Inc., 11034 Crescent Drive, Nevada City, CA 95959, USA
(2) Department of Architecture, Built Environment and Construction Engineering, Politecnico di Milano, Piazza Leonardo da Vinci, 32, 20133 Milan, Italy.
* Corresponding author: gabriele.milani@polimi.it

Abstract. This work proposes a novel non-destructive, vision-based measurement strategy to identify and quantify mechanical deformations between rigid blocks. First the possible motions between two rigid blocks were identified and measured, under the application of a perpendicular, parallel and symmetrical 4x4 point grid around the masonry joint line. Repeated calculations of lengths, dot products, and right triangles improved the precision of measurements through redundancy. Then, this method was verified via photographic images with defined deformation and 2D holography, showing good adaptability and precision. Finally, this strategy was performed to a video recording of an arch under tilting test until failure. With the dimensions of the points grid being the only known parameter, the mechanical joint, the type of rigid block motion, the failure point and the rotation angle were successfully determined.

1. Introduction

Efficient and economical experimental measurements can help structural engineers to better understand structural behavior and develop guidelines to establish reliable engineering projects. In this article, the discussion will be limited to the measurements on masonry arches, which are not only very common in architectural heritages, but are also proposed as an alternative framing system to reinforced concrete and steel [1]. The typical failure of an arch is mechanical and reversible, providing the possibility for implementing structural health monitoring (SHM) systems [2,3].

Non-destructive testing (NDT) plays an important role in both existing building monitoring and new construction. One NDT approach that has been employed for masonry arches is vision-based techniques, such as photogrammetry, digital image correlation (DIC), and laser scanning [4-6], due to the advantages of low cost, easy setup and operation, and the flexibility to extract information [7]. However, the computation costs increase as these approaches become more refined and it's still difficult to achieve real-time health monitoring of the structure. In this paper, the failure identification and deformation calculation can be greatly simplified based on the 2D homography [8], under the consideration of 4 hinges mechanism for masonry arch.

This work presents an NDT strategy for mapping the deformation of a masonry arch by measuring the movement of joints, which is realized through a novel approach that records the displacement of a 4x4 point grid around the joint. Compared with other vision-based measuring techniques, this proposed method does not have demanding requirements for camera position and video quality, meanwhile only a small amount of information and calculations are needed for post-processing which allows potential use of security cameras for near real-time monitoring. This article introduces the identification and

calculation of joint deformations, which were fully validated by photographic images with known deformations. Then this strategy was successfully applied to a masonry arch under tilting platform capacity test.

2. Calculation principles and verification

2.1. Deformation identification and calculations

2.1.1 Deformation identification. For a masonry arch based on stability-based design, the rigid-no-tension model, and under the assumption of maintaining contact there will be eight possible deformations between two blocks in the propagation of failure, including rotation, slip and combinations of the two. Figure 1 demonstrates all eight deformations, and provides the mathematical relationships to identify the deformation type by the relative displacement of the points in the grid. The orignal distance is indicated without any superscript as l, while the deformed distance is indicated with l' for a single kind of deformation (slip or rotation), and with l'' for combined deformation. The difference between oringal and deformed distance Δ is defined as

$$\begin{cases}\Delta l_{i23} = l'_{i23} - l_{i23} \\ \Delta l'_{i23} = l''_{i23} - l'_{i23}\end{cases} \tag{1}$$

where subscript i stands for the serial number of row (a, b, c or d), $k_{l'_{a23}}$ is the slope of line l'_{a23}.

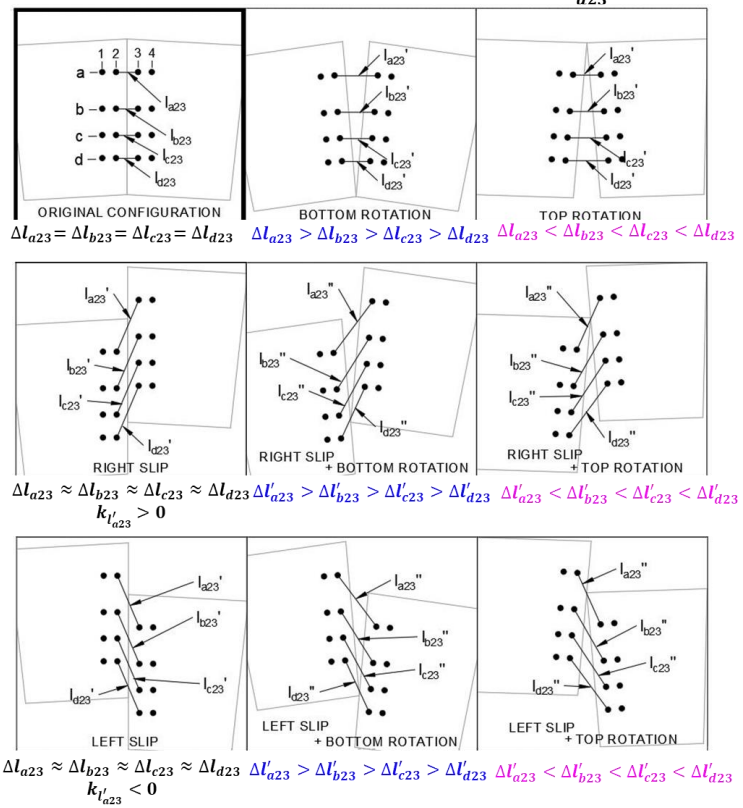

Figure 1. Eight deformations of arch joints and the corresponding identification methods

To identify the different two types of slip, the slop of line

2.1.2 Deformation calculations. Assume that the original point grid is parallel, normal and symmetric to the joint line. One way to determine the rotation angle is through the dot product of two vectors before and after deformation:

$$\begin{cases}\alpha = \theta_L + \theta_R \\ \theta = cos^{-1}\left(\dfrac{l'_{jkl} \cdot l_{jkl}}{\|l'_{jkl}\| \|l_{jkl}\|}\right)\end{cases} \tag{2}$$

where θ_L and θ_R are the rotation angle on the two sides of the joint. And the subscript *j* stands for the column (or row) number, the subscripts *k* and *l* stand for two points in the j^{th} column (or row) at the same side of joint.

The second approach is directly through the dot product of the deformed condition:

$$\alpha = \cos^{-1}\left(\frac{l'_{jkl}\cdot l'_{mkl}}{\left\|l'_{jkl}\right\|\left\|l'_{mkl}\right\|}\right) \quad (3)$$

where the subscript *j* and *m* stand for two columns on the opposite sides of the joint line (that is on two blocks separately). To calculate with points along rows, the rotation angle is

$$\alpha = \cos^{-1}\left(\frac{l'_{jkl}\cdot l'_{jno}}{\left\|l'_{jkl}\right\|\left\|l'_{jno}\right\|}\right) \quad (4)$$

where the subscript *j* stands for the row number, the subscript *k* and *l* stand for points on the rows of left block (the 1st row and 2nd row as indicated in Figure 1), and the subscript *n* and *o* stand for points on the rows of right block (the 3rd row and 4th row).

The slip displacements, δ, can be measured by the right triangle established between the original and deformed configuration of a pair of symmetrical points about the joint line

$$\delta = \sqrt{\left(l'_{jkl}\right)^2 - \left(l_{jkl}\right)^2} \quad (5)$$

where the subscript *j* stands for the row number, the subscripts *k* and *l* stand for two symmetric points in the 2nd and 3rd columns (or 1st and 4th columns) separately.

In the case where slip and rotation are combined, the slip always occurs before rotation under previous assumptions. Thus, the slip can be calculated by equation (5) without considering any rotation, and the rotation can still be gained by the dot product regardless of the translational deformation.

2.1.3 Redundancy. Angle calculations are extremely sensitive to measurement precision. The strategy proposed above easily overcomes this problem through redundancy. Based on equation (2), for each column, there will be six combinations of the four points, thus generating 24 different distances to calculate α of the 4x4 point grid. For each row, there will be eight more combinations. Similarly, equation (3) will generate 24 values of α, and four more values from equation (4). In total, 60 calculations for the rotation angle α can be performed, and if the precision of the point locations is uniform, these 60 calculated measurements can increase the angle precision by 7.7.

The calculation for length is less sensitive with respect to rotation. From equation (5), eight calculations can be conducted which can increase the precision of slip by 2.8 under uniform measurement error.

2.2. Validation of the measurement strategy

2.2.1 Identifying Point Sets The reliability of this strategy was verified through the photographic images of joints with known deformations. A rotation angle of 10° and a slip of 4.30 cm was applied for the deformation conditions. To ensure that the camera position and lens type did not affect the measurements, photos were taken from three different viewpoints. The process was repeated for all eight deformations. An image processing script was developed in MATLAB® to convert photos to binary images as shown in Figure 2.

2.2.2 Two-dimensional homography transformation. For a rigid block, the surface will remain plane. This allows the plane to be determined by the points. The points can be projected from one plane to another plane via a homography transformation:

$$\begin{bmatrix} x' \\ y' \\ 1 \end{bmatrix} = H \begin{bmatrix} x \\ y \\ 1 \end{bmatrix} \quad (6)$$

where, *H* is the 3x3 homography matrix which maps the points (x, y) from one coordinate system onto another coordinate system, (x', y'), through control point pairs [9]. This homography matrix can be constructed through the *fitgeotrans* function provided in MATLAB®. The control point pairs adopted in this analysis are the known measured distances of points on each block. From Figure 2, it can be

recognized that the transformations procedure successfully projects the points from a photo onto a cartesian plane.

Utilizing the aforementioned calculations and redundancy, the error of the rotation angles from the accurate value (10°) is less than 1° in all views and deformations, and the precision is between 2 to 4 digits for every case. The slip calculation results are very consistent, and each obtains three digits of precision. Considering the quite short time required of this calculation (less than one second), it can be said that this simple method can efficiently and precisely track the deformed arch in near-real time.

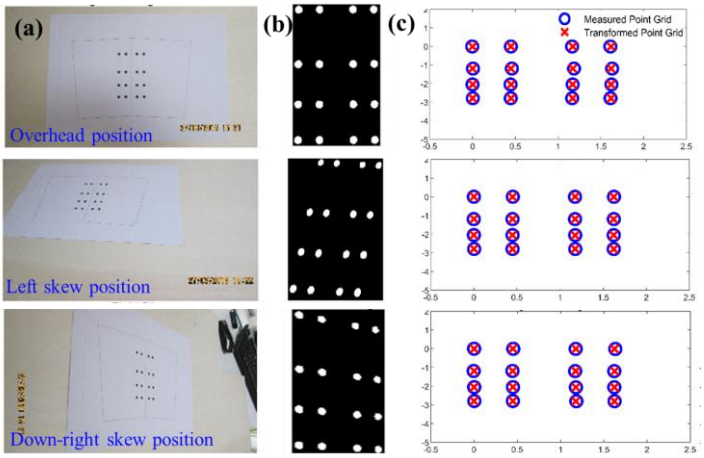

Figure 2. (a) Original joint points configuration under different views, (b) identification and (c) comparisons of measured and transformation positions

3. Application to experimental observations

3.1. Experimental overview

The proposed strategy was applied to a previous experimental campaign aimed at determining the capacity of a hinge-controlled masonry arch subjected to a tilting plane [10]. A semi-circular arch composed of 27 blocks was constructed with oriented standard boards and steel risers. Then 4x4 point grids were applied around the joints, as shown in Figure 3(a). Note that the joints were numbered from 1 to 27 from right to left of the arch. The failure of the arch was caused by the horizontal acceleration induced through the quasi-static tilting of the platform. For each test, the four mechanical joints were achieved by the absence of reinforcement. All other joints were reinforced with a combination of double-sided Velcro and cam straps. During the tests, videos were taken. The position and type of camera was considered in the analysis since the information does not affect the implementation of the proposed strategy.

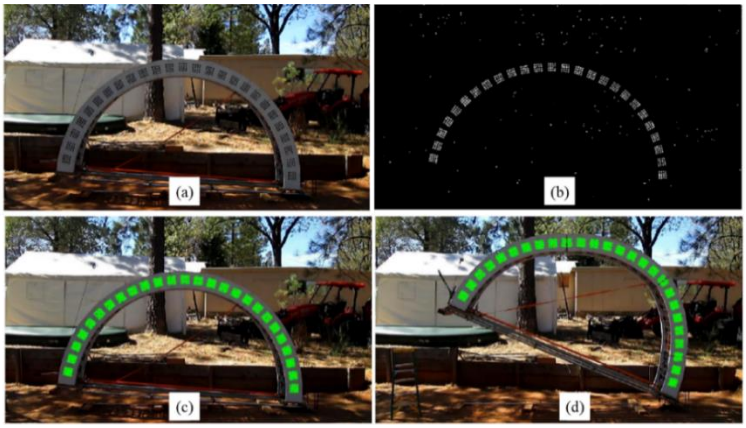

Figure 3. Identifying and tracking of points: (a) The first frame of the video; (b) Binary mask treatment; (c) First frame for tracking;(d) Final frame when mechanism formed.

3.2. Point tracking

The tracking of the points was realized via MATLAB® Computer Vision Toolbox [11]. The first step was to identify the 4x4 grid points of the 27 joints by their centroids. A binary mask for the first frame of the video was created as shown in Figure 3(b) to achieve this. Then through the geometric recognition of the arch and grids, the noise was eliminated and the needed points determined in their respective sets. These points were then carried through each frame by creating a binary mask and evaluating the assignment cost between the defined points and those of the mask. In this way, the point tracking in the video was achieved. The assignment cost referred to the length between the object centroids in the two frames before and after. At the same time, a sequence was created to record the position data of every tracking point. With the known template point distances, the coordinates were transformed via the 2D homography approach introduced above.

3.3. Identifying mechanical joints

For each frame of the video, the distance of four pairs of points were averaged to eliminate the errors caused by low image resolution. Two sets of paired points are calculated, denoted as outer points (points in the 1st and 4th columns) and inner points (points in the 2nd and 3rd columns). The two average lengths versus frame number were plotted (see Figure 4), to check the accuracy of point tracking and transformation, and to determine the mechanical joints of the arch through the increase in lengths when deformation initiated. As shown in Figure 4, the trend of distance increment is quite clear, and the noises can be easily eliminated by standard spline or least squares fitting with a polynomial objective function. By comparing all plots of the 27 joints, joints 3, 9, 17, and 22 can be clearly identified as mechanical joints due to obvious length increases when compared to other joints. It can also be determined that joint 3 and joint 17 behaved as top rotations while joint 9 and joint 22 were bottom rotations. The rotation angles were also obtained via the calculations presented in Section 2.1.

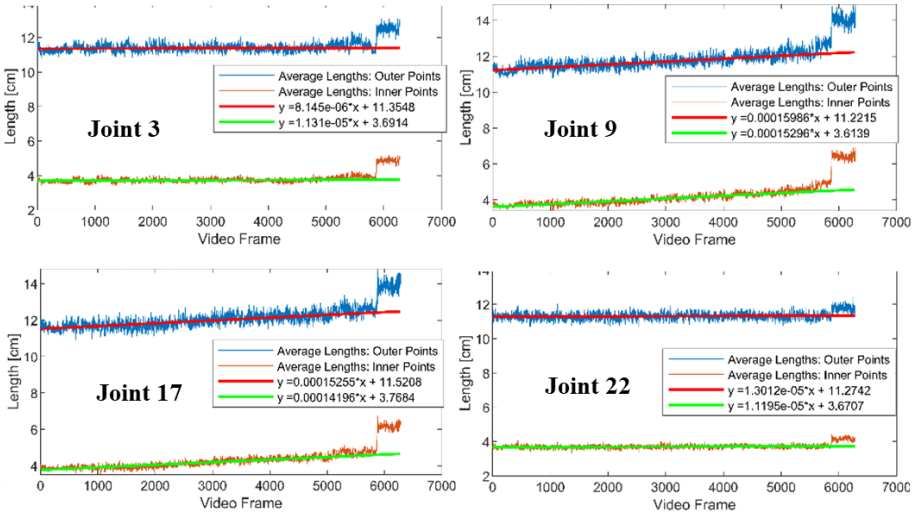

Figure 4. Average point pair lengths versus frame number for mechanical joints

4. Conclusions

This work presented a novel non-destructive, vision-based method to identify and quantify the mechanical deformations between rigid blocks. First, the possible eight motions between two rigid blocks were discussed. It is described how to use a 4x4 point grid to identify and quantify the motion, and to improve the accuracy through the calculation redundancy. This approach was then validated by photographic images taken from different views with known deformation and 2D holography transformation. Finally, the measurement method was performed to a video recording of an arch under tilting plane test. The centroids of marked points around the joint line were identified and recorded in the first frame, then tracked via MATLAB® code through the whole video. Based only on the knowledge of the dimensions of the points grid, the proposed approach can identify the mechanical joints, the type

of deformation, and the angle of joint rotation. Although the application results on the masonry arch showed a positive judgment that this strategy is quite convenient, efficient and accurate, there is still room for improvement. The accuracy of point tracking can be improved by increasing the contrast between the grids and the surroundings, or using non-visible reflective materials like infrared and ultraviolet, or refining signal processing techniques and statistical analysis methods.

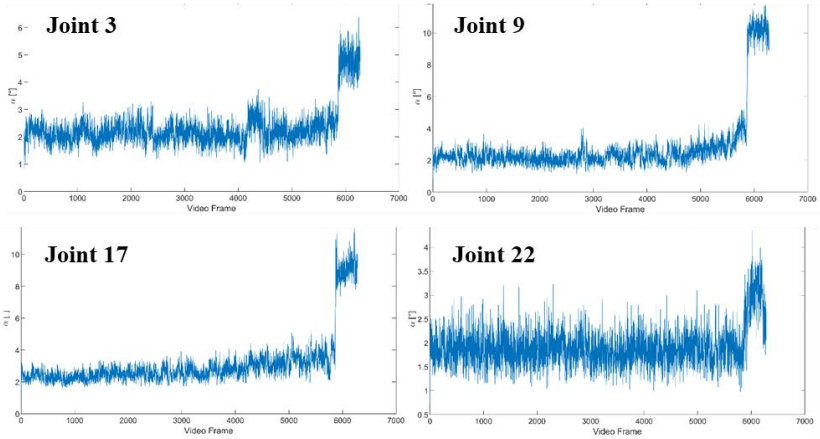

Figure 5. Calculated rotation angle versus frame number for mechanical joints

References

[1] G.L. Stockdale, Reinforced stability-based design: a theoretical introduction through a mechanically reinforced masonry arch, Int. J. Mason. Res. Innov., 1:2 (2016) 101–142.

[2] N. Grillanda, G. Milani, S. Ghosh, B. Halani, M. Varma, SHM of a severely cracked masonry arch bridge in India: Experimental campaign and adaptive NURBS limit analysis numerical investigation, Construction and Building Materials, 280 (2021) 122490. https://doi.org/10.1016/j.conbuildmat.2021.122490.

[3] G. Stockdale, Generalized Processing of FBG/FRP Stain Data for Structural Health Monitoring. Master's Thesis. University of Hawai'i at Mānoa, Honolulu, HI, USA (2012).

[4] Riveiro B, Caamaño J C, Arias P, et al. Photogrammetric 3D modelling and mechanical analysis of masonry arches: An approach based on a discontinuous model of voussoirs[J]. Automation in Construction, 2011, 20(4): 380-388.

[5] Ghorbani R, Matta F, Sutton M A. Full-field deformation measurement and crack mapping on confined masonry walls using digital image correlation[J]. Experimental Mechanics, 2015, 55(1): 227-243.

[6] Lubowiecka I, Arias P, Riveiro B, et al. Multidisciplinary approach to the assessment of historic structures based on the case of a masonry bridge in Galicia (Spain)[J]. Computers & structures, 2011, 89(17-18): 1615-1627.

[7] Feng D, Feng M Q. Computer vision for SHM of civil infrastructure: From dynamic response measurement to damage detection–A review[J]. Engineering Structures, 2018, 156: 105-117.

[8] M. Shafiei Dizaji, M. Alipour, D.K. Harris, Leveraging Full-Field Measurement from 3D Digital Image Correlation for Structural Identification, Experimental Mechanics. 58 (2018) 1049–1066. doi:10.1007/s11340-018-0401-8.

[9] R. Hartley, A. Zisserman, Multiple View Geometry in Computer Vision, Cambridge University Press, (2004). doi:10.1017/CBO9780511811685.

[10] G.L. Stockdale, G. Milani, V. Sarhosis, Increase in Seismic Resistance for a Full-Scale MasonryArch Subjected to Hinge Control, Key Engineering Materials, (2019) 221-228. https://doi.org/10.4028/www.scientific.net/KEM.817.221.

[11] R. Szeliski, Computer Vision, Springer London, London, (2011). doi:10.1007/978-1-84882-935-0.